RSC Advances

ROYAL SOCIETY OF CHEMISTRY

www.rsc.org/advances

RSC Advances

RSCPublishing

ARTICLE

Galvanic replacement-mediated synthesis of hollow Cu_2O-Au nanocomposites and Au nanocages for catalytic and SERS applications

Cite this: DOI: 10.1039/x0xx00000x

Received 00th January 2012,
Accepted 00th January 2012

DOI: 10.1039/x0xx00000x

www.rsc.org/

Lu Xiong,[‡a] Siwei Li,[‡b] Bin Zhang,[*a] Peng Miao,[a] Yan Ma,[a] Yingxin Han,[a] Hongtao Zhao,[a] and Ping Xu[*a]

Galvanic replacement reaction (GRR) involves a corrosion process that is driven by the difference in the electrochemical potentials of two species. Here we demonstrate the synthesis of hollow Cu_2O-Au nanocomposites *via* a GRR process between Cu_2O and $HAuCl_4$, and subsequent conversion of the hollow Cu_2O-Au nanocomposites into Au nanocages that are actually assembled by ~10 nm Au nanoparticles. It is interesting to find that Cu_2O nanocubes produced from reductive solution chemistry are actually transformed from $Cu(OH)_2$ nanowire precursors, and the Cu_2O particle size is inversely proportional to the reaction temperature. Time-dependent TEM study of the GRR process between Cu_2O and $HAuCl_4$ indicates that this reaction involves evolution of an internal hollow core and surface precipitation of Au nanoparticles, which allows the formation of hollow Cu_2O-Au nanocomposites. Comparing the properties of hollow Cu_2O-Au nanocomposites and Au nanocages, it is determined that the hollow Cu_2O-Au nanocomposites are more catalytically active in the reduction of 4-nitrophenol into 4-aminophenol in the presence of $NaBH_4$, and Au nanocages are two orders of magnitude more sensitive in SERS detection of the target molecule, methylene blue. We believe the findings in this work may render a better understanding of the preparation and GRR process of Cu_2O nanomaterials.

Introduction

Galvanic replacement reaction (GRR) has received more and more attention in preparing metal and metal oxide (sulfide) nanoparticles with controllable size, shape and properties,[1-5] where a corrosion process that is driven by the difference in the electrochemical potentials of two species is involved. GRR method allows selective deposition onto oxidizable structures, without the need of an external voltage and a reducing agent. Based on the chemical nature of the sacrificing template, GRR can lead to metal/metal oxide heterojunctions, metal nanoparticles, and even oxide/oxide nanostructures.[4, 6-10] In recent years, many sacrificing templates have been found to be suitable in the GRR, such as Cu_2O, Mn_3O_4, MnO, Ag. For instance, Lee, et al.[11] reported a GRR-based Pt deposition on Mn_3O_4 NPs through reaction between Mn_3O_4 and $PtCl_4^{2-}$ complexes, and the obtained Pt/Mn_3O_4 showed excellent oxygen reduction reaction properties. They also used carbon-encapsulated MnO nanoparticles or a Mn_3O_4-layer-coated interior surface of the hollow silica nanosphere as a reaction template for the selective decoration of the external surfaces with catalytic nanocrystals of various noble metals, including Pt, Pd, Rh, and Ir.[10, 12] Ag nanoparticles have been widely used as sacrificing templates to fabricate various metal and metal alloy nanostructures,[13-21] which can be applied in catalysis, imaging, and therapy, etc. Cu_2O has been widely used in GRR to produce functional metal nanoparticles and metal/oxide hybrid nanocomposites.[22] Liu, et al.[23] reported an *in situ* growth of Au NPs on the surfaces of Cu_2O nanocubes. Rubinstein and co-workers systematically studied the pH-dependent galvanic replacement of supported and colloidal Cu_2O nanocrystals with gold and palladium.[2] In our previous work,[6] self-supported Pt nanoclusters consisting of 2-3 nm NPs were synthesized *via* a GRR process between Cu_2O and $PtCl_4^{2-}$ and we pointed out the

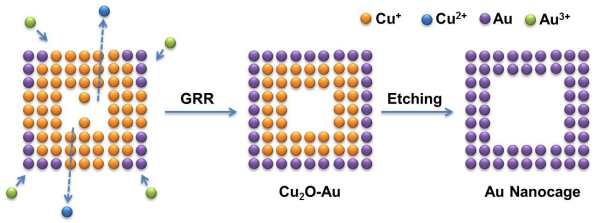

Scheme 1 Schematic illustration of the synthesis of hollow Cu_2O-Au nanocomposites and Au nanocages through a galvanic replacement reaction (GRR) process between Cu_2O and $HAuCl_4$.

importance of solution acidity for the GRR to proceed, where Cu_2O was transformed into Cu^{2+} ions and surface-clean Pt electrocatalysts can be achieved. Ag nanosheet or nanoparticle assemblies could be prepared *via* reaction between Ag^+ ions and Cu_2O substrates, which show promise as surface-enhanced Raman scattering (SERS) substrates.[7, 24]

Herein, we demonstrate the fabrication of hollow Cu_2O-Au nanocomposites by careful control over the GRR process between Cu_2O and $HAuCl_4$, and then conversion of the as-prepared hollow Cu_2O-Au nanocomposites into Au nanocages by an acid etching process (Scheme 1). The evolution of Cu_2O nanocubes from $Cu(OH)_2$ nanowire precursors has been found out, and the GRR process between Cu_2O and $HAuCl_4$ has been investigated by time-dependent TEM study. It is determined that the hollow Cu_2O-Au nanocomposites and Au nanocages show different properties in catalytic and SERS applications. We believe this work may open new avenues for the synthesis of metal/oxide and metal nanostructures *via* GRR process for various applications.

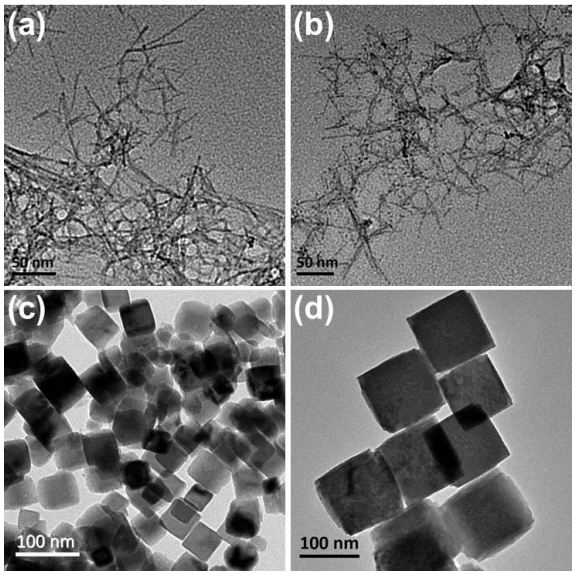

Fig. 1 TEM images of $Cu(OH)_2$ nanowire precursors prepared at room temperature (a) and in ice-water bath (b), and Cu_2O nanocubes prepared at room temperature (c) and in ice-water bath (d).

Experimental section

Synthesis of Cu_2O nanocubes. Cu_2O nanocubes were prepared through a modified reductive solution chemistry route.[25,26] In a typical procedure, 0.5 g of poly(ethylene glycol) (PEG, MW:2000) was first dissolved in 10 mL of $Cu(Ac)_2$ aqueous solution (0.1 mM). Once PEG was completely dissolved, 50 μL of NaOH solution (6.0 M) was added dropwise. Upon addition, the solution immediately changed to blue color, indicating the formation of $Cu(OH)_2$ precursors. After 10 min, 0.2 ml of ascorbic acid (AA) solution (1 M) was added dropwise to the solution, where the solution slowly turned into orange color. The products were collected by centrifugation after a reaction time of 1 h by repeatedly rinsing with DI water and ethanol in order to minimize the surface adsorbed PEG molecules. Here, the experiments were carried out at room temperature or in ice-water bath to study the effect of temperature in the growth of Cu_2O nanocubes.

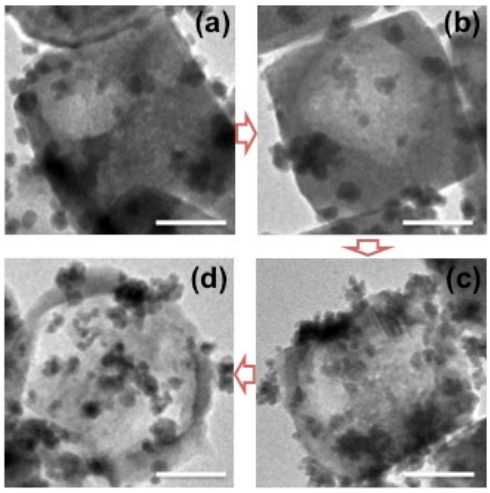

Fig. 2 Time-dependent TEM study of the galvanic replacement process between Cu_2O and $HAuCl_4$, (a) 30 sec, (b) 1 min, (c) 2 min, and (d) 5 min. Scale bar: 50 nm.

Synthesis of hollow Cu_2O-Au nanocomposites and Au nanocages. Synthesis of hollow Cu_2O-Au nanocomposites and Au nanocages was achieved through a galvanic replacement process between Cu_2O and $HAuCl_4$. For the synthesis of hollow Cu_2O-Au nanocomposites, 40 mg of as-synthesized Cu_2O nanocubes were ultrasonically re-dispersed in deionized water, and then 40 mL of $HAuCl_4$ solution (1mM) was added under magnetic stirring. The reaction was maintained for 5 min before the hollow Cu_2O-Au nanocomposites were collected by centrifugation and rinsing with water and ethanol. For the synthesis of Au nanocages, 60 mL of $HAuCl_4$ solution (1mM) were used to prepare Cu_2O-Au nanocomposites with more Au loading. Then, the as-prepared hollow Cu_2O-Au nanocomposites were re-dispersed into 30 mL deionized water, followed by adding 10 mL of HCl (0.01 M) to dissolve the Cu_2O. Stirring was not applied in order not to destroy the nanocage framework. The products were collected by centrifugation and rinsing with water and ethanol.

Catalytic reduction of 4-nitrophenol. The reduction of 4-nitrophenol was carried out in the presence of $NaBH_4$ in a quartz cuvette and monitored by UV-Vis spectroscopy at room temperature.[27] A total 60 μL of 4-nitrophenol aqueous solution (10 mM) was mixed with 0.16 mL of fresh $NaBH_4$ (0.1 M) solution. Subsequently, 0.1 mL of hollow Cu_2O-Au nanocomposites or Au nanocages dispersion (catalyst content: 1 mg/mL) was added, and the mixture solution was quickly subjected to UV–Vis measurements to record the change in absorbance at a time interval of 1 min.

SERS measurements. Methylene blue (MB) dye was used as a Raman probe for the SERS sensitivity of the hollow Cu_2O-Au nanocomposites and Au nanocages. Typically, aqueous

dispersion of hollow Cu_2O-Au nanocomposites or Au nanocages was injected into MB aqueous solution with variable concentrations ranging from 1.0×10^{-5} M to 1.0×10^{-9} M. After 1 h, the resulting mixture solution was centrifuged and re-dispersed on glass substrate and dried in air before the surface-enhanced Raman scattering (SERS) responses were determined.

Characterization. Powder X ray diffraction (XRD) patterns of the samples were obtained on an XRD-6000 (Shimadzu) using a Cu Kα source (λ=0.154056 nm). Transmission electron microscope (TEM, Tecnai G2 F20) and Scanning electron microscope (SEM, FEI Quanta 200F) were applied to observe the particle size and surface morphology. The SERS spectra were recorded on a Renishaw In Via micro Raman spectroscopy system, using the TE air-cooled 576×400 CCD array in a confocal Raman system (wavelength: 633 nm).

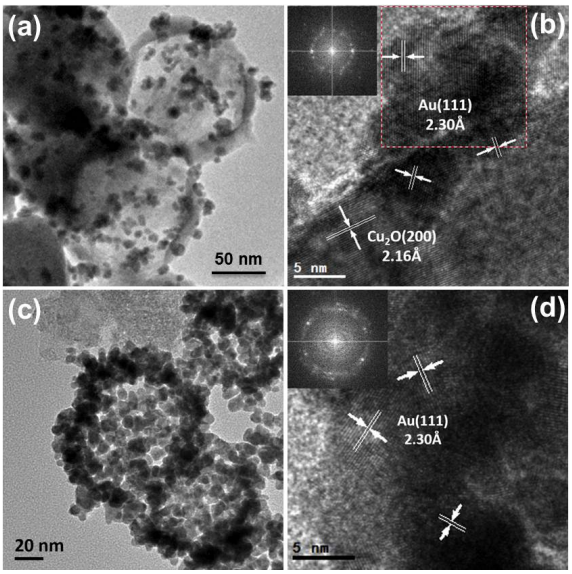

Fig. 3 TEM and HR-TEM images of Cu_2O-Au nanocomposites (a, b) and Au nanocages (c, d) prepared from a galvanic replacement process between Cu_2O and $HAuCl_4$.

Results and discussion

Preparation of Cu_2O through the reductive chemistry route mainly involves two reactions: precipitation of Cu^{2+} ions with OH^- ions into $Cu(OH)_2$ precursor, and reduction of $Cu(OH)_2$ into Cu_2O by ascorbic acid (AA). In our previous work, we have demonstrated that different surfactants applied in the reaction system could lead to Cu_2O nanoparticles with various nanostructures.[25] Here, we investigated the reaction process by TEM study of the $Cu(OH)_2$ precursor and Cu_2O product, and found that the reaction temperature could also manipulate the Cu_2O particle size. As shown in Fig. 1 a and b, the blue $Cu(OH)_2$ precursors obtained at room temperature and in ice-water bath are similar nanowires that are about 5-10 nm in diameter. Interestingly, these $Cu(OH)_2$ nanowires are subsequently transformed into Cu_2O nanocubes during the reductive process (Fig. 1 c and d). Of note is that here we found that a lower temperature condition leads to Cu_2O nanocubes with larger size: 40-60 nm at room temperature (Fig. 1 c) *vs* 100-120 nm in ice-water bath condition (Fig. 1 d). This inverse relationship between reaction temperature and particle size might be interpreted from the nucleation and growth of Cu_2O from $Cu(OH)_2$ through the interfacial reduction. At a relatively high temperature, reaction between $Cu(OH)_2$ and AA follows a rapid process, leading to more crystal nuclei and thus Cu_2O nanoparticles with smaller size during the subsequent growth stage. While, at low temperature, a slow reaction process between $Cu(OH)_2$ and AA produces limited nuclei, and Cu_2O can grow into larger nanoparticles. Actually, higher temperature leading to Cu_2O nanoparticles with smaller size has been seen in the growth of Cu_2O@CeO_2 core@shell nanocubes.[28] However, the evolution of Cu_2O nanocubes from $Cu(OH)_2$ nanowires has not been reported previously and the underlying mechanism remains to be explored.

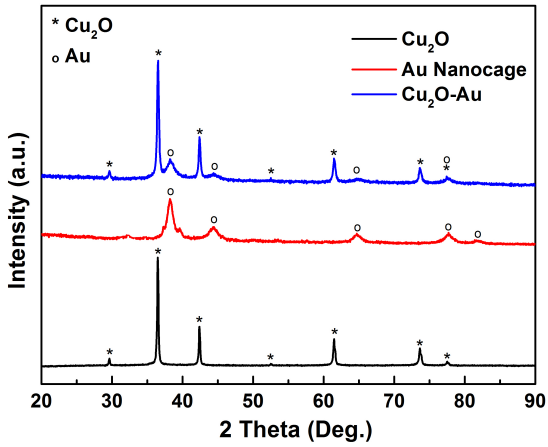

Fig. 4 X-ray diffraction (XRD) patterns of the as-prepared Cu_2O nanocubes, Cu_2O-Au nanocomposites and Au nanocages.

Galvanic replacement reaction (GRR) between Cu_2O and $HAuCl_4$ follows the reaction,

$$3Cu_2O + 6H^+ + 2AuCl_4^- \rightarrow 2Au + 6Cu^{2+} + 8Cl^- + 3H_2O \quad (1)$$

and this reaction follows a very rapid process, as the orange color of Cu_2O nanocubes will be immediately changed into dark brown upon interaction with $HAuCl_4$. And we found that the structure of Cu_2O nanocubes that are 40-60 nm in size (Fig. 1 c) can be easily destroyed, and only scattered Au nanoparticles can be obtained (See Fig. S1 in ESI†). Therefore, here we used the Cu_2O nanocubes that are 100-120 nm in size (Fig. 1 d) to study the galvanic replacement process between Cu_2O and $HAuCl_4$ (Fig. 2), and this reaction involves evolution of an internal hollow core and surface precipitation of Au nanoparticles. It can be seen that the inside part of the Cu_2O nanocubes will be firstly etched by a mechanism analogous to pinhole corrosion, and the pinholes serve as transport paths during the dissolution of Cu_2O nanocubes. With the elongation of reaction time, hole expansion and Au precipitation result in hollow Cu_2O-Au nanocomposites. However, given long enough reaction time and adequate $HAuCl_4$ source, the Cu_2O will be fully dissolved and the nanocube framework will be eventually

collapsed, resulting in only dispersed Au nanoparticles (See Fig. S2 in ESI†). It has been reported that reaction between $HAuCl_4$ and Cu_2O might lead to CuO,[22] but we found Cu_2O would be transformed into soluble Cu^{2+} species in acidic environment.[6]

Before the Cu_2O is completely dissolved, it is easy to get hollow Cu_2O-Au nanocomposites (Fig. 3 a and b), which consist of 5-10 nm Au nanoparticles and internal hollow Cu_2O. From the HR-TEM image in Fig. 3 b, one can clearly see that Au nanoparticles grown along the (111) plane are decorated on the Cu_2O surface. As mentioned above, without experimental control, the Cu_2O nanocube framework will be eventually collapsed and only dispersed Au nanoparticles are produced. Here, we used an acid etching technique to obtained well-defined Au nanocages (Fig. 3 c and d), where more $HAuCl_4$ is used to increase the Au loading. The obtained Cu_2O-Au nanocomposites were then re-dispersed into water and subject to HCl etching to remove the Cu_2O. It is interesting that the framework of the nanocubes is not destroyed and the obtained Au nanocages are comprised of an assembly of ~10 nm Au nanoparticles, and the size of the nanocage is similar to that of the Cu_2O nanocubes. HR-TEM image of the Au nanocages shows that these highly crystallized Au nanoparticles are also grown mainly along the (111) plane. The hollow Cu_2O-Au and Au nanocage structures can also be confirmed from the SEM studies (See Fig. S3 in ESI†). Therefore, by careful control of the galvanic replacement process, we are able to get hollow Cu_2O-Au nanocomposites and Au nanocages.

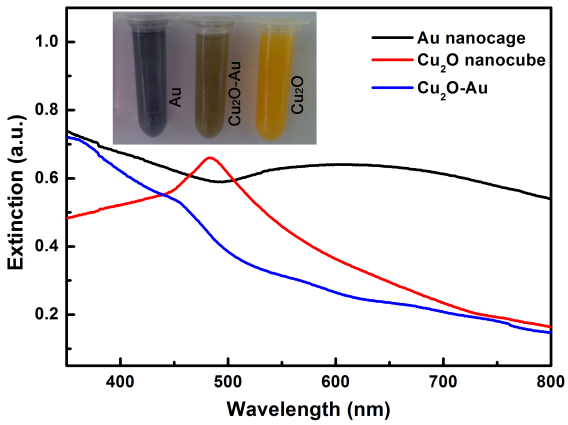

Fig. 5 Extinction spectra of Cu_2O nanocubes, hollow Cu_2O-Au nanocomposites, and Au nanocages. Inset shows the optical images of these samples dispersed in water.

The successful formation of Cu_2O-Au nanocomposites and subsequent transformation into Au nanocages can be confirmed by the X-ray diffraction (XRD) patterns in Fig. 4. The diffraction peaks appeared at 2θ=~29.6, 36.5, 42.4, 52.6, 61.5, 73.7 and 77.6° (labeled with *) in the Cu_2O nanocubes can be well indexed to the (110), (111), (200), (211), (220), (311), and (222) crystal planes of the Cu_2O crystals in cubic phase (PDF No. 65-3288), indicating the production of pure Cu_2O samples, without any CuO or $Cu(OH)_2$ impurities. Besides the diffraction peaks of Cu_2O in the Cu_2O-Au nanocomposites, one can also see diffraction peaks at 2θ=~38.2, 44.6, 64.7, and 77.5°, corresponding to the (111), (200), (220), (311) crystal planes (labeled with °) of face-center-cubic (fcc) Au crystals (PDF No. 01-1172). After acid etching, the Cu_2O can be completely removed and only diffraction peaks of Au can be seen in the as-prepared Au nanocages.

From the optical images inset in Fig. 5, one can see that the as-prepared Cu_2O nanocubes are orange in color, and the hollow Cu_2O-Au nanocomposites become dark brown. While the Au nanocages, which are about 100 nm in size and assembled by tiny nanoparticles, display darkish blue color. Extinction spectra of these samples dispersed in water are also determined. The Cu_2O nanocubes that are 100-120 nm in size show an absorption peak at about 485 nm, which agrees well with the previous reports.[26] The Au nanocages that are ~100 nm in size have a very broad absorption band centered at ~610 nm. Different from reported Au nanocages that usually show strong absorption at ~800 nm,[29] here we think the red shift of the absorption peak can be interpreted by the fact that the prepared Au nanocages are actually assembled by ~10 nm nanoparticles (Fig. 3c). While, it is interesting to see that the extinction spectrum of the hollow Cu_2O-Au nanocomposites differs a lot from that of Cu_2O nanocubes and Au nanocages, where no distinct absorption peak can be detected. We think this can be understood through the TEM studies (Fig. 2 and 3), where very limited Cu_2O remains in the Cu_2O-Au nanocomposites during the galvanic replacement process. Moreover, aggregation of Au nanoparticles on the remained Cu_2O frameworks to give the new hollow Cu_2O-Au nanocomposites may also cause this phenomenon. An absorption shoulder at ~ 560nm can well reflect the size of Au nanoparticles supported on the hollow Cu_2O edges.[3] A dynamic light scattering (DLS) study of the Cu_2O-Au nanocomposites and Au nanocages shows that they are quite stable in solution, and the size distribution agrees well with the TEM results (See Fig. S4 in ESI†).

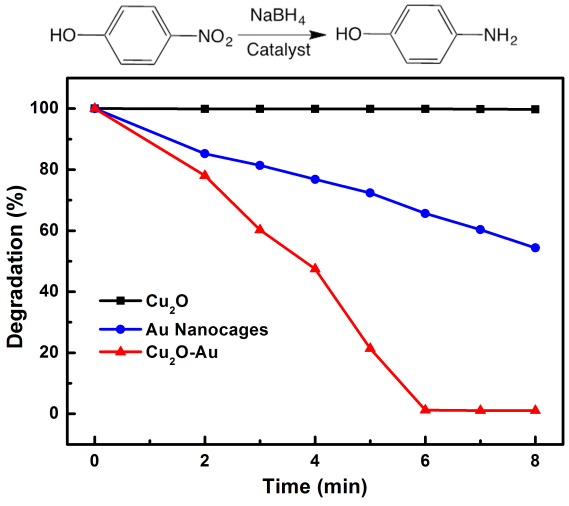

Fig. 6 Catalytic performance of reduction of 4-nitrophenol into aminophenol in the presence of $NaBH_4$ using Cu_2O nanocubes, hollow Cu_2O-Au nanocomposites, and Au nanocages as catalysts.

Au nanoparticles are promising catalysts for various chemical reactions and assemblies of Au nanoparticles are suitable for chemical detection based on surface enhanced Raman spectroscopy (SERS).[30-33] Here, we tested the properties of the as-prepared hollow Cu_2O-Au nanocomposites and Au nanocages in catalytic reduction of 4-nitrophenol in the presence of $NaBH_4$ and SERS detection of methylene blue (MB). The reduction of 4-nitrophenol into 4-aminophenol can be monitored by the absorption peak at about 405 nm in the UV-Vis spectroscopy (See Fig. S5 in ESI†). As shown in Fig. 6, the as-prepared 100-120 nm Cu_2O nanocubes almost have no catalytic effect to the reduction of 4-nitrophenol. The hollow Cu_2O-Au nanocomposites are highly efficient for this reaction, as the 4-nitrophenol can be fully converted into 4-aminophenol at a time scale of 6 min. Surprisingly, the Au nanocages are less effective in catalyzing this reaction, since only ~55% of 4-nitrophenol are reacted after 8 min. Aggregation of Au nanoparticles usually occurs during the catalytic process in solution, which will decrease the catalytic activity and cycling performance. Therefore, many works have been focused on the fabrication of Au nanoparticles on various carriers, which can effectively reduce the aggregation and thus maintain the catalytic activity.[34-36] Here, we think the Au nanoparticles supported on hollow Cu_2O nanostructures are more active in catalyzing this reaction, and Au nanocages, which are essentially an assembly of Au nanoparticles, may suffer from particle aggregation through Ostward ripening and reduction of surface area during the reaction process (See Fig. S6 in ESI†).

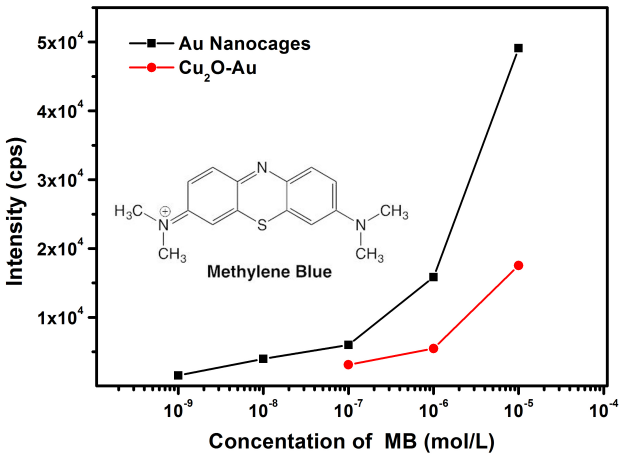

Fig. 7 Concentration-dependent Raman intensity of the ν(C−C) ring stretching at 1618 cm^{-1} of methylene blue (MB) using hollow Cu_2O-Au nanocomposites and Au nanocages as SERS substrates.

It is interesting to find that as compared with the catalysis study, hollow Cu_2O-Au nanocomposites and Au nanocages have an inverse effect in SERS detection, where Au nanocages are more sensitive and promising as SERS platforms. With methylene blue (MB) as the target molecule, well-resolved Raman fingerprints can be distinguished on both hollow Cu_2O-Au nanocomposites and Au nanocages (See Fig. S7 in ESI†). However, Au nanocages can be two orders of magnitude more sensitive in SERS detection. As shown in Fig. 7, with the Raman intensity of the ν(C−C) ring stretching at 1618 cm^{-1} of MB as a reference, a detection limit of 10^{-7} M was found on hollow Cu_2O-Au nanocomposites, which can be as low as 10^{-8} M on Au nanocages. Moreover, at the same concentration of MB, the Raman intensity is much stronger on Au nanocages, an indication that Au nanocages are more suitable as a SERS platform for chemical detection. This can be explained from the SERS image of the two samples, where more hot spots with stronger Raman intensity can be detected on an aggregation of Au nanocages (See Fig. S8 in ESI†). This clearly shows that the Au nanoparticle assemblies in the nanocages can generate more hot spots for SERS detection, since the gaps and junctions between two adjacent Au nanoparticles are usually favorable to create much enhanced electromagnetic fields.[37] In order to show the generality of Au nanocages for SERS detection, we have used another molecule, Thiram, one kind of pesticides as an analyte. It was found that the detection limit of Thiram could also reach 10^{-9} M on Au nanocages (See Fig. S9 in ESI†). SERS response in the NIR region has been of great interest, and it might be of great interest to test the SERS performances of the as-prepared materials if NIR laser sources are available.[38]

Conclusions

In conclusion, we have demonstrated here the structural evolution of Cu_2O nanocubes in reductive solution chemistry route and the synthesis of hollow Cu_2O-Au nanocomposites and Au nanocages *via* a controlled galvanic replacement reaction (GRR) process. Cu_2O nanocubes are transformed from $Cu(OH)_2$ nanowire precursors, and the size of Cu_2O nanocubes shows an inverse relationship with the reaction temperature. The GRR process between Cu_2O and $HAuCl_4$ follows a mechanism analogous to pinhole corrosion, allowing the formation of hollow Cu_2O-Au nanocomposites. Au nanocages are then obtained by an acid etching treatment to remove the Cu_2O of the hollow Cu_2O-Au nanocomposites. The hollow Cu_2O-Au nanocomposites, with Au nanoparticles well dispersed on the Cu_2O framework, are promising catalyst for the reduction of 4-nitrophenol in the presence of $NaBH_4$. On the contrary, Au nanocages, formed by an assembly of 10 nm Au nanoparticles, are more sensitive in chemical detection based on SERS technique, due to the generation of more hot spots by gaps and junctions between two adjacent Au nanoparticles. We believe the findings in this work may be intended to the synthesis of hollow nanostructures for various applications.

Acknowledgements

We thank the support from NSFC (No. 21471039, 21203045), Fundamental Research Funds for the Central Universities (Grant No. HIT. NSRIF. 2010065 and 2011017, PIRS of HIT A201502, and HIT.BRETIII. 201223), China Postdoctoral Science Foundation (2013M541394, 2014M560253 and 2014T70341), Natural Science Foundation of Heilongjiang

Province (B2015001), Heilongjiang Postdoctoral Fund (LBH-Z14076), and Postdoctoral Scientific Research Developmental Fund of Heilongjiang Province (LBH-Q14062).

Notes and references

[a] State Key Laboratory of Urban Water Resource and Environment, Harbin Institute of Technology, Harbin 150001, China.
Email: pxu@hit.edu.cn; zhangbin_hit@aliyun.com.
[b] College of Chemistry and Molecular Engineering, Peking University, Beijing 100871, China.

† Electronic Supplementary Information (ESI) available: Fig. S1-S9. See DOI: 10.1039/b000000x/
‡ These two authors contributed equally to this work.

1. E. Sutter, K. Jungjohann, S. Bliznakov, A. Courty, E. Maisonhaute, S. Tenney and P. Sutter, *Nat Commun*, 2014, **5**, 4946.
2. M. D. Susman, R. Popovitz-Biro, A. Vaskevich and I. Rubinstein, *Small*, 2015, DOI: 10.1002/smll.201500044.
3. S. E. Skrabalak, J. Y. Chen, Y. G. Sun, X. M. Lu, L. Au, C. M. Cobley and Y. N. Xia, *Accounts Chem Res*, 2008, **41**, 1587-1595.
4. M. H. Oh, T. Yu, S. H. Yu, B. Lim, K. T. Ko, M. G. Willinger, D. H. Seo, B. H. Kim, M. G. Cho, J. H. Park, K. Kang, Y. E. Sung, N. Pinna and T. Hyeon, *Science*, 2013, **340**, 964-968.
5. E. Gonzalez, J. Arbiol and V. F. Puntes, *Science*, 2011, **334**, 1377-1380.
6. Q. Li, P. Xu, B. Zhang, G. Wu, H. T. Zhao, E. G. Fu and H. L. Wang, *Nanoscale*, 2013, **5**, 7397-7402.
7. W. Jin, P. Xu, L. Xiong, Q. Jing, B. Zhang, K. Sun and X. J. Han, *Rsc Adv*, 2014, **4**, 53543-53546.
8. B. E. Dixon, M. Rosenman, Y. N. Xia and S. J. Grannis, *Stud Health Technol*, 2013, **192**, 884-888.
9. W. Yao, F. L. Li, H. X. Li and J. P. Lang, *J Mater Chem A*, 2015, **3**, 4578-4585.
10. D. G. Lee, S. M. Kim, H. Jeong, J. Kim and I. S. Lee, *Acs Nano*, 2014, **8**, 4510-4521.
11. K. W. Kim, S. M. Kim, S. Choi, J. Kim and I. S. Lee, *Acs Nano*, 2012, **6**, 5122-5129.
12. S. M. Kim, M. Jeon, K. W. Kim, J. Park and I. S. Lee, *J Am Chem Soc*, 2013, **135**, 15714-15717.
13. L. Au, X. M. Lu and Y. N. Xia, *Adv Mater*, 2008, **20**, 2517-+.
14. V. Bansal, A. P. O'Mullane and S. K. Bhargava, *Electrochem Commun*, 2009, **11**, 1639-1642.
15. M. H. Cao, L. Zhou, X. Q. Xu, S. Cheng, J. L. Yao and L. J. Fan, *J Mater Chem A*, 2013, **1**, 8942-8949.
16. J. Y. Chen, B. Wiley, J. McLellan, Y. J. Xiong, Z. Y. Li and Y. N. Xia, *Nano Lett*, 2005, **5**, 2058-2062.
17. X. Y. Liu, A. Q. Wang, L. Li, T. Zhang, C. Y. Mou and J. F. Lee, *Prog Nat Sci-Mater*, 2013, **23**, 317-325.
18. X. M. Lu, H. Y. Tuan, J. Y. Chen, Z. Y. Li, B. A. Korgel and Y. N. Xia, *J Am Chem Soc*, 2007, **129**, 1733-1742.
19. C. X. Wang, Y. Wang, L. Xu, X. D. Shi, X. W. Li, X. W. Xu, H. C. Sun, B. Yang and Q. Lin, *Small*, 2013, **9**, 413-420.
20. Y. Yang, J. Y. Liu, Z. W. Fu and D. Qin, *J Am Chem Soc*, 2014, **136**, 8153-8156.
21. C. Zhang, Y. Zhang, D. K. Yao, Y. N. Xia and L. H. V. Wang, *Photons Plus Ultrasound: Imaging and Sensing 2012*, 2012, **8223**.
22. M. L. Pang, Q. X. Wang and H. C. Zeng, *Chem-Eur J*, 2012, **18**, 14605-14609.
23. X. W. Liu, F. Y. Wang, F. Zhen and J. R. Huang, *Rsc Adv*, 2012, **2**, 7647-7651.
24. T. Gao, Y. Q. Wang, K. Wang, X. L. Zhang, J. N. Dui, G. M. Li, S. Y. Lou and S. M. Zhou, *Acs Appl Mater Inter*, 2013, **5**, 7308-7314.
25. Q. Li, P. Xu, B. Zhang, H. Tsai, S. J. Zheng, G. Wu and H. L. Wang, *J Phys Chem C*, 2013, **117**, 13872-13878.
26. L. F. Gou and C. J. Murphy, *J Mater Chem*, 2004, **14**, 735-738.
27. F. H. Lin and R. A. Doong, *J Phys Chem C*, 2011, **115**, 6591-6598.
28. X. Wang, D. P. Liu, J. Q. Li, J. M. Zhen and H. J. Zhang, *Npg Asia Mater*, 2015, **7**, e158.
29. J. Chen, F. Saeki, B. J. Wiley, H. Cang, M. J. Cobb, Z. Y. Li, L. A H. Zhang, M. B. Kimmey, X. D. Li and Y. N. Xia, *Nano Lett*, 2005, **5**, 473-477.
30. B. Zhang, B. T. Zhao, S. H. Huang, R. Y. Zhang, P. Xu and H. L. Wang, *Crystengcomm*, 2012, **14**, 1542-1544.
31. W. Y. Li, J. G. Liu and C. W. Yan, *Carbon*, 2013, **55**, 313-320.
32. H. Zhu, M. L. Du, D. L. Yu, Y. Wang, L. N. Wang, M. L. Zou, M. Zhang and Y. Q. Fu, *J Mater Chem A*, 2013, **1**, 919-929.
33. J. Zeng, Q. Zhang, J. Y. Chen and Y. N. Xia, *Nano Lett*, 2010, **10**, 30-35.
34. J. Li, C. Y. Liu and Y. Liu, *J Mater Chem*, 2012, **22**, 8426-8430.
35. Q. M. Ji, J. P. Hill and K. Ariga, *J Mater Chem A*, 2013, **1**, 3600-3606.
36. J. W. Xie, W. Y. Liu, M. R. MacEwan, P. C. Bridgman and Y. N. Xia, *Acs Nano*, 2014, **8**, 1878-1885.
37. P. Xu, N. H. Mack, S. H. Jeon, S. K. Doorn, X. J. Han and H. L. Wang, *Langmuir*, 2010, **26**, 8882-8886.
38. H. N. Xie, I. A. Larmour, Y. C. Chen, A. W. Wark, V. Tileli, D. W. McComb, K. Faulds and D. Graham, *Nanoscale*, 2013, **5**, 765-771.

